Published in final edited form as:
Acta Biomater. 2010 January ; 6(1): 110–122. doi:10.1016/j.actbio.2009.06.026.

A Bi-Layered Elastomeric Scaffold for Tissue Engineering of Small-Diameter Vascular Grafts

Lorenzo Soletti[1,3,4,5], **Yi Hong**[3,4,5], **Jianjun Guan**[3,4,5], **John J. Stankus**[2,4], **Mohammed S. El-Kurdi**[1,3,4,5], **William R. Wagner**[1,2,3,4,5], and **David A. Vorp**[1,3,4,5]

[1]University of Pittsburgh, Department of Bioengineering, Pittsburgh, PA 15219

[2]University of Pittsburgh, Department of Chemical Engineering, Pittsburgh, PA 15219

[3]University of Pittsburgh, Department of Surgery, Pittsburgh, PA 15219

[4]University of Pittsburgh, McGowan Institute for Regenerative Medicine, Pittsburgh, PA 15219

[5]University of Pittsburgh, Center for Vascular Remodeling and Regeneration Pittsburgh, PA 15219

Abstract

A major barrier in the development of a clinically-useful small-diameter tissue engineered vascular graft (TEVG) is the scaffold component. Scaffold requirements include matching the mechanical and structural properties with those of native vessels and optimizing the microenvironment to foster cell integration, adhesion, and growth. We have developed a small-diameter, bi-layered, biodegradable, elastomeric scaffold based on a synthetic, biodegradable elastomer. The scaffold incorporates a highly porous inner layer, allowing cell integration and growth, and an external, fibrous reinforcing layer deposited by electrospinning. Scaffold morphology and mechanical properties were assessed, quantified, and compared to those of native vessels. Scaffolds were then seeded with adult stem cells via a rotational vacuum seeding device to obtain a TEVG, cultured in dynamic conditions for 7 days, and evaluated for cellularity. The scaffold showed a firm integration of the two polymeric layers with no delaminations. Mechanical properties were physiologically-consistent showing anisotropy, elastic modulus (1.4±0.4 MPa), and ultimate tensile stress (8.3±1.7 MPa) comparable with native vessels. Compliance and suture retention force were $4.6\pm0.5\times10^{-4}$ $mmHg^{-1}$ and 3.4±0.3 N, respectively. Seeding resulted in a rapid, uniform, bulk integration of cells, with a seeding efficiency of 92±1%. The scaffolds maintained a high level of cellular density throughout dynamic culture. This approach, combining artery-like mechanical properties and a rapid and efficient cellularization, might contribute to the future clinical translation of TEVGs.

Keywords

Vascular tissue engineering; tubular scaffold; polymer processing; cell seeding; poly(ester urethane)urea; electrospinning

1. Introduction

Cardiovascular disease remains the leading cause of mortality in western nations with an estimated prevalence of almost 80 million in the United States alone [1]. In particular,

Address for Correspondence and Reprints: David A Vorp, PhD, 100 Technology Drive, Suite 200, Pittsburgh, PA, 15219 Phone: 412-235-5136 Fax: 412-235-5110 VorpDA@upmc.edu.

coronary artery disease is the leading cause of death, counting for 53% of the total mortality related to cardiovascular disease [1]. Despite significant improvements in our understanding of coronary artery disease, and the broad adoption of minimally invasive treatments such as balloon angioplasty and stenting, the therapeutic gold standard for high risk patients remains the coronary artery bypass graft (CABG) [2]. Together with CABG, other non-cardiac bypass vascular procedures, such as lower limb revascularization and arteriovenous fistula for hemodialysis access, account for more than 1 million cases per year [1, 3, 4]. Such procedures rely on the availability of healthy autologous vessels, which are not ideal [5], and have limited availability and associated donor-site morbidity. Efforts toward developing bio-durable, synthetic, small-diameter vascular grafts have been hampered by poor biocompatibility at the blood-biomaterial interface and mechanical mismatch, which leads to graft failure and recurrent disease [6, 7]. Regenerative medicine and, in particular, tissue engineering approaches are being investigated as potential solutions to these problems [8].

The fundamental difference between traditional vascular grafts and tissue engineered vascular grafts (TEVGs) based on scaffolds is biodegradation of the scaffold material used. TEVGs thus depend on the capacity of donor- and host-derived cells to secrete and remodel the scaffold, concurrently replacing it with extracellular matrix (ECM) into a native-like structure. Several attempts have been made to produce a TEVG [8] including the use of decellularized native blood vessels [9], cell-hydrogel suspensions based on biological proteins [10, 11], synthetic scaffolds seeded with cells [12, 13], and sheets of cells wrapped around a mandrel [14]. While each of these previous methods have their merits, to date there is no clear consensus as to what approach – past, present, or future – might lead to a clinically-applicable treatment. Most of the limitations of previous approaches have involved the lack of appropriate matching of mechanical properties to those of native arteries [15] which could lead to rupture in case of insufficient strength or compliance mismatch in case of high stiffness, the long time frames required to achieve necessary mechanical or biological characteristics [16], and/or the poor cellularity of the TEVG [17].

Critical to the majority of vascular tissue engineering approaches is the scaffold component [18], which as a temporary 3-D template provides structural, mechanical and possibly biological support and guidance throughout the tissue formation and remodeling processes. Foremost, the scaffold should allow for cell infiltration, adhesion, and proliferation, followed by cell-mediated remodeling leading to ECM deposition [19]. Other requirements for the scaffold include mechanical strength, compliance and suture retention strength comparable to physiologic values [20]. Moreover, the scaffold should not possess significant plastic behavior since this could lead to aneurysm formation upon long-term implantation. Toward a more “biomimetic” approach the scaffold should hypothetically possess structural and mechanical properties similar to native bloods vessels [21, 22].

Biodegradable polyurethanes represent attractive potential candidate biomaterials for use in TEVG scaffold construction due to their elasticity and tunable mechanical and degradation properties. A class of biodegradable polymers based on poly(ester-urethane)urea (PEUU) [23] has recently been developed. PEUUs have been shown to be cytocompatible, yield non-toxic degradation products, and to be processable into scaffolds via various techniques [23-25]. A thermally-induced phase separation (TIPS) process has been used to produce highly porous scaffolds [24]. This process can yield a morphology promoting efficient cell integration, cell attachment, and diffusion of nutrients allowing for culture *in vitro* [12, 26]. Electrospinning (ES) is a different processing technique, which can yield sub-micron fibrous PEUU with architectural and mechanical properties similar to those of native elastic ECM [25]. Indeed, it was demonstrated that by varying the rotational speed of the ES target that the degree of structural anisotropy and associated mechanical properties could be reproducibly and predictably controlled [27]. More recently, the challenge of evenly

distributing cells throughout the thickness of these relatively small-pored ES scaffolds has been largely overcome by a novel process termed “cellular microintegration” in which cells and PEUU are co-deposited [28, 29]. Collectively, the above-mentioned flexibilities of PEUU chemistry and processing techniques made available a plethora of permutations from which to choose and combine in designing a new scaffold for vascular tissue engineering applications.

In the current study, the TIPS and ES processes were applied sequentially to obtain a composite (*i.e.*, bi-layered) tubular scaffold. By this new approach, desirable microstructural and mechanical characteristics yielded by TIPS and ES, respectively, were rationally integrated for the purpose of designing a novel scaffold for small-diameter vascular tissue engineering applications. Two different diameters (1.3 mm internal diameter (ID) and 4.7 mm ID) were produced that would be appropriate for in subsequent assessment of these scaffolds in a rat infrarenal aortic interposition graft and pig carotid interposition graft, respectively. Morphological and mechanical characterization was performed to test compatibility of the scaffold relative to the native vasculature. The mechanical properties of the composite scaffold were compared to those of its two scaffold components (*i.e.*, TIPS and ES PEUU) individually, and to those of native human saphenous veins (hSVs) and porcine internal mammary arteries (pIMAs). The scaffolds were then bulk-seeded with muscle-derived stem cells (MDSCs) isolated from skeletal muscle, which exhibit multipotentiality including the ability to differentiate toward vascular lineages, self-renewal capabilities, and have a direct role in tissue remodeling and regeneration both *in vitro* and *in vivo* [30-32]. Their multipotentiality may obviate the need for endothelial cell seeding with primary cells, although such a verification is beyond the aims of the present investigation. MDSCs have been used by our group in our previous efforts toward the development of a viable TEVG and its culture *in vitro* [12], and to assess the efficiency of cell inclusion within a short seeding time in a study using a rotational vacuum seeding device [26]. Finally, the seeded scaffolds were cultured in dynamic culture conditions for up to 7 days to assess cell spreading and proliferation into the developed scaffold.

2. Materials and Methods

2.1. Polymer synthesis

Polycaprolactone diol (PCL, Aldrich, number average molecular weight = 2000) was dried under vacuum for 48 h at 50°C. Solvent dimethyl sulfoxide (DMSO) was dried over 4-A molecular sieves. Putrescine (Sigma) and 1,4-diisocyanatobutane (BDI, Fluka) were distilled under vacuum. Stannous octoate (Sigma) catalyst and 1,1,1,3,3,3-hexafluoroisopropanol (HFIP, Oakwood) solvent were used as received. PEUU was synthesized from BDI and PCL with putrescine chain extension as described previously [23]. Synthesis proceeded as a solution polymerization with DMSO using a 2:1:1 BDI:PCL:putrescine molar ratio.

2.2. Scaffold preparation

Two different small-diameter composite scaffolds types were made, both a larger (ID-4.7; length = 30 mm, ID = 4.7 mm), and smaller (ID-1.3; length = 10 mm, ID = 1.3 mm) diameter. The two scaffold sizes were chosen to be suitable for implantation in a large animal model (juvenile pig) as a carotid interposition graft, or in a small animal model (adult Lewis rat) as an abdominal aortic interposition graft, respectively. A previous morphometric analysis based on histological samples obtained from unrelated animal studies was performed (data not shown) to obtain the average values used as internal diameter for the two scaffold sizes. The internal layer (*i.e.*, intima/media equivalent) of the composite scaffolds consisted of porous PEUU, obtained using TIPS as previously described [24]. Briefly, PEUU solutions in DMSO (5% w/v) were poured at 80°C into custom-made molds,

accordingly dimensioned for the two different scaffold sizes. Each mold consisted of an internal stainless steel (for the ID-4.7 mold) or tungsten carbide mandrel (for the ID-1.3 mold) covered by poly(tetrafluoroethylene) (PTFE) tubing. The mandrels were concentrically aligned into a tubular glass sheath using two custom-machined PTFE sealing stoppers. The molds were filled with hot polymer solution, then rapidly cooled to −80°C for 3 h. The molds were subsequently uncapped and immersed in 70% ethanol for 1-2 weeks at 4°C to remove the solid solvent crystals, yielding an interconnected pore structure. The scaffolds were washed for 48 h in deionized water to remove residual solvent, and freeze-dried for an additional 48 h. The TIPS conduits were subsequently coated by ES of PEUU using an apparatus and technique previously described [25]. Briefly, the TIPS conduits were slipped onto mandrels (diameters: 4.0 mm or 1.0 mm) in conjunction with an intermediate sleeve made of PTFE tubing to facilitate insertion and removal. PEUU solution in HFIP (8% w/w) [33] was prepared and loaded into 10 mL syringes connected via plastic tubing to a steel capillary (ID = 1.2 mm), which was suspended 7 cm over the target TIPS tubular scaffold/mandrel. The mandrels were rotated at 250 rpm and simultaneously translated on an x-y stage (Velmex Inc., Bloomfield, NY) along the longitudinal direction of the mandrels in a cyclic manner (translational speed = 6 cm/s, amplitude = 8 cm, frequency = 0.4 Hz). The mandrels were charged with −3 kV, while the capillary was charged with 10 kV. High voltage was supplied for each component using a combination of two high voltage generators (Gamma High Voltage Research, Ormond Beach, FL). The polymer solution was infused via a precision syringe pump (Harvard Apparatus, Holliston, MA) at 1 mL/h. A schematic of the process is shown in Figure 1. The ES time for the 4.7 mm-ID scaffold was 1 h, while for the 1.3 mm-ID it was 15 min. At the end of the process, electrospun polymer deposited beyond the extension of the underlying TIPS scaffold was removed with a razor. The scaffolds were dried within a vacuum chamber for 24 h. Sterilization was performed by immersing the scaffolds in 70% ethanol solution for 24 h followed by multiple washes with sterile Dulbecco's modified phosphate buffered saline (DPBS).

2.3. Morphological assessment

ES-TIPS PEUU scaffolds were immersed in liquid nitrogen and rapidly cut with a cold razor to generate a sharp fracture, exposing a cross-section with preserved structural features. The specimens were mounted dry on aluminum stubs with double adhesive copper tape and sputter coated with gold (Sputter Coater 108 auto, Cressington Scientific Instruments Inc., Cranberry Twp., PA) with a 3.5 nm thick layer of gold. The cross-sections were imaged by field emission scanning electron microscopy (JSM-6330F, JEOL ltd. Tokyo, Japan). Image-based analysis (ImageJ) was used to measure the thickness of the two layers, the dimension of the pores, and the thickness of the ES fibers. A total of 10 to 30 measurements were used for each scaffold analyzed (n = 3). Pore size was measured as the maximum diameter of all void spaces visible in the image.

2.4. Mechanical properties

2.4.1. Uniaxial test—Mechanical testing was performed only on the ID-4.7 conduits due to size limitations with the ID-1.3 scaffolds. To measure uniaxial material properties of the scaffolds, a tensile tester (Tytron TM250, MTS System Corp., Minneapolis, MN) mounted with a 10 lb force transducer (Model 661.11B-02, MTS System Corp., Minneapolis, MN) was used. Dry scaffolds were cut into strips (width ~2 mm, length ~15 mm) along their circumferential or longitudinal directions. Adjacent samples were cut in paraffin blocks to retrieve accurate thickness measurements of each specimen with image-based techniques. To ensure a firm but delicate retention of the scaffold within the metal tensile system clamps, each specimen was mounted via a sandwich of thin cardboard and hot glue [34]. Specimen length and width were measured with a digital caliper (Thermo Fisher Scientific, Waltham, MA). The dry specimens from each direction were tested at room temperature by

pulling at 10 mm/min crosshead speed until rupture following 10 cycles of preconditioning to 20% strain. Load–displacement curves were computed to obtain stress–strain relationships according to current length and cross-sectional area with the assumption of incompressibility, as previously described [29]. Ultimate tensile stress (UTS) and strain to failure (STF) were considered, respectively as the maximum stress value before failure and its corresponding value of strain. Elastic modulus was estimated by calculating the slope of the stress-strain curves for the level of circumferential strain measured while pressurizing the scaffold at arterial physiologic pressures.

hSVs were obtained from discarded portions of vein grafts used in CABG procedures and tested following protocols compliant with the University of Pittsburgh Institutional Review Board. pIMAs were harvested from animals used for unrelated acute surgical studies. These native vessels were tested uniaxially only in the circumferential direction following a slightly different experimental setup (*i.e.*, ring test [29]). This was due to size limitations with the native vessels and the difficulty in establishing a firm grip of the wet and slippery native tissue as was achieved for the dry scaffolds. Briefly, to measure ring strength, an ATS uniaxial tensile tester (10 mm/min crosshead speed according to ASTM D638-98 until sample failure) mounted with a 10 lb force transducer (SM-10, Interface) was modified to surround the two clamps with a custom-fabricated sealed chamber filled with saline. A recirculation circuit composed of a roller pump, Tygon® tubing, and heat exchanger was constructed in order to maintain a constant temperature of 37°C during the tests. A ring (1-2 mm length) of each vessel specimen was cut and the diameter, thickness, and width were measured with a dial caliper. The rings were inserted with two custom-made stainless steel flat hooks that were subsequently attached to the clamps of the testing device. All specimens were preconditioned prior to testing with 10 cycles at 5% circumferential stretch. Load-displacement curves were computed as previously described [29] to obtain stress-strain relationships. The stress-strain relationships were derived to calculate the instantaneous elastic modulus.

2.4.2. Burst strength—Burst pressure was measured by pressurizing the scaffolds and the native vessels with compressed air while immersed in a saline bath maintained at 37°C via a heat exchanger. The scaffold samples were first loaded internally with high viscosity freezing medium (TBS, Triangle Biomedical Sciences), which has negligible mechanical properties, to clog the pores, avoiding transluminal flow of air for complete pressure retention [29]. Air was infused at 100 mL/min as previously described [21] and pressure was measured via a high pressure gauge (pressure range = 0-60 PSI, Noshok, Berea, OH) after clamping the downstream line. The maximum pressure before rupture was taken as the burst pressure.

2.4.3. Suture retention strength—Suture retention testing for scaffolds and native vessels was performed according to American National Standard Institute-Association for the Advancement of Medical Instruments (ANSI/AAMI) VP20 standards [14] using the same two testing apparatuses as for the uniaxial testing. Briefly, each tubular sample was cut to obtain rectangular strips (n = 4, length = 10 mm, width = 4 mm) with the short edge of each specimen belonging to the circumference of the original tubular scaffold. A single 5-0 PDS™ (Ethicon, Inc.) loop was created 2 mm from the short edge of each sample and secured to a hook connected to the clamp of the testing device. An extension rate of 2 mm/sec was used to pull the suture. Scaffolds were tested in dry state while native vessels were tested in saline at 37°C. Suture retention strength was considered to be the maximum force recorded prior to pull–through of the suture. Suture retention tension was obtained by normalizing the suture retention strength to the thickness of each scaffold.

2.4.4. Dynamic compliance—Dynamic compliance measurements were performed using a previously described vascular perfusion system [35]. The flow loop was filled with saline maintained at 37°C, and delivered physiologic, arterial, pulsatile intraluminal pressure (120/80 mmHg) and flow (100 mL/min). Briefly, a Biomedicus centrifugal pump connected with Tygon® tubing to a testing chamber, produced sinusoidal pulsatile pressure and flow consistent with physiologic values. Two pressure transducers (Model TJE, Honeywell – Sensotec Co., Columbus, OH) placed equidistant upstream and downstream of the vessel center were used to measure intraluminal pressure. The pressure in the center of the vessel was then calculated as the average between the proximal and distal pressure transducer measurements. The outer diameter of the pressurized scaffolds was measured with a He-Ne laser micrometer (Beta LaserMike, Dayton, OH). Both pressure and diameter signals were automatically recorded at 30 Hz for 1 min every hour over 24 h using an acquisition card connected to a personal computer. Compliance, *C*, was calculated from recordings of pressure, *P* and inner diameter, ID_p as:

$$C=\frac{(ID_{120}-ID_{80})}{ID_{80}}\frac{1}{P_{120}-P_{80}} \quad (1)$$

Where P_{120} = 120 mmHg and P_{80} = 80 mmHg. The inner diameter, ID_p, was estimated with an assumption of incompressibility from the cross sectional area, *A*, of the scaffold (measured from histological sections of the same construct using ImageJ software), and the outer diameter OD_p of the scaffold (measured with a laser micrometer) by the expression:

$$ID_p=2\cdot\sqrt{\left(\frac{OD_p}{2}\right)^2-\frac{A}{\pi}} \quad (2)$$

Recordings of OD_p for each time point were also used to calculate the percentage of scaffold dilation over time ($\Delta D_{\%}$) to quantify possible plastic deformations due to creep. This value was calculated by dividing the average pressurized external diameter at each time point by the initial average pressurized external diameter for each tested scaffold. Pressure-diameter relationships during static compliance measurements were also used to compute the dimensionless stiffness index, β:

$$\beta=\frac{\ln\left(\frac{P_{120}}{P_{80}}\right)}{\left[\frac{(OD_{120}-OD_{80})}{OD_{80}}\right]} \quad (3)$$

2.5. Cell seeding

Both scaffold sizes were bulk-seeded using a previously described rotational vacuum seeding device (RVSD) allowing fast (1-5 min) and uniform integration of cells [26]. Briefly, the RVSD is comprised of an airtight chamber holding two coaxial tees mechanically coupled by a torque transmission component to allow for simultaneous tee rotation. The chamber is connected to a vacuum line by a pneumatic resistive circuit to maintain a negative relative pressure within it during seeding. The tees are externally connected to a syringe pump by means of hydraulic rotating joints and Tygon® tubing. The seeding device takes advantage of the synergistic actions of vacuum applied inside the chamber and the flow generated by the syringe pump to induce a transmural flow through the porous polymer scaffold mounted on the two tees. During this phase, the cells infused by the syringe become entrapped within the pores of the scaffold while the liquid phase of the cell suspension exudes through it. The rotation of the tubular scaffold inside the chamber

during the seeding increases the uniformity of seeding along its circumferential direction. Different scaffolds, IDs and lengths can be mounted into the same device by utilizing a variety of custom-made tee adaptors accounting for different scaffold IDs, and by modifying the gap between the two tees to account for different scaffold lengths.

Rat muscle-derived stem cells (MDSCs) obtained from an established pre-plating technique and characterized as described previously [32] were used as they represent a promising alternative for vascular tissue engineering applications [12], and may circumvent many of the shortcomings associated with other options in cell sourcing, including the limited availability of fully differentiated cells. MDSCs were expanded in Dulbecco Modified Eagle Medium (DMEM; Sigma) supplemented with 1% penicillin/streptomycin (Gibco, Invitrogen Corporation, Carlsbad, CA), 10% fetal calf serum (Atlanta Biologicals, Norcross, GA), and 10% horse serum (Gibco, Invitrogen Corporation). The seeding was performed using serum-free medium. Different cell numbers were used for the two scaffolds corresponding to an equivalent seeding density of approximately 1.5×10^5 cells/mm^3 (*i.e.*, 3×10^6 cells for the ID-1.3 and 30×10^6 cells for the ID-4.7 scaffolds, respectively). The scaffolds were seeded under a vacuum of −130mmHg, and either an infusion rate of 2.5 mL/min and a rotational speed of 150 rpm (for the ID-1.3 scaffolds), or an infusion rate of 4 mL/min and a rotation speed of 10 rpm (for the ID-4.7 scaffolds). Immediately after the seeding of each sample, the media exuded through the scaffold into the RVSD chamber was collected and used for cell counting with a hematocytometer to calculate seeding efficiency (percentage of the initial cell number entrapped within the scaffolds). The scaffolds were then placed in static culture in Petri dishes for 2 h. Subsequently, a small ring was cut from each scaffold and fixed in 4% paraformaldehyde for 1 h. After washing in PBS, the specimens were embedded in tissue freezing medium (TBS, Triangle Biomedical Sciences, Durham, NC) and sectioned with a cryostat (Cryotome, from both scaffold sizes were permeabilized in Triton-X-100 solution (Fisher Scientific, Fair Lawn, NJ) for 15 min and F-actin filaments were stained with a 1:250 dilution of phalloidin conjugated to Alexa 488 (Molecular Probes, Eugene, OR) for 1 h. Sections from both scaffold sizes were counter-stained with the nuclear stain, DAPI (bisbenzimide, Sigma) for 1 min. The sections were observed with epifluorescence microscopy using an Eclipse E800 microscope (Nikon Instech Co., Ltd., Kanagawa, Japan) with a UV filter for the DAPI stain and with a FITC filter for the phalloidin stain. The scaffold itself was visualized with high exposure times (~10 sec) under TRITC filter.

2.6. TEVG culture and viability

In a separate experiment, ID-1.3 scaffolds were seeded and cultured statically for 2 h as described for the previous seeding assessment, and subsequently placed into spinner flasks (196580575, Bellco Glass Inc., NJ) at 15 rpm for 7 days. Constructs were assessed for F-actin and nuclear staining immediately after the 2 h of static culture, and after 3 and 7 days of dynamic culture. The cell density, proliferation, and spreading into the ES-TIPS scaffold were quantified with an image-based technique. In particular, nuclear staining images were taken at 10× magnification and processed with the ImageJ software. Proper image scaling was performed by analyzing the dimensions of a reference microscale. Grayscale images were thresholded and subsequently processed with a watershed filter to identify and separate overlapping nuclei. The number of nuclei was automatically counted with a particle counting function. The cell density was obtained by dividing the measured scaffold area by the counted number of nuclei. The F-actin area was obtained by threshholding images obtained with the FITC filter and by measuring the resulting total area. Cell spreading was quantitatively estimated by measuring the area of F-actin staining and dividing it by the number of counted nuclei in each image. Merged images were used to evaluate the results qualitatively at each time point.

2.7. Statistical methods

All statistical analyses were performed using SPSS v.15 software (SPSS Inc., Chicago, IL). All datasets were tested for normality using the Shapiro-Wilk test. Comparison of the mean values of the data sets was performed using one-way ANOVA. Post hoc analysis was performed with the Bonferroni test. Measures are presented as mean ± standard deviation, unless otherwise specified. A p-value less than 0.05 was considered significant.

3. Results

3.1. Morphological assessment

ES-TIPS PEUU scaffolds appeared macroscopically smooth and without any gross defects (Figure 2-A). Observed under SEM, the scaffolds exhibited a morphology characterized by two distinct layers: a highly porous internal layer (TIPS) and a fibrous external layer (ES) (Figures 2 and 3). The measured thickness of the TIPS layer in the ID-1.3 and the ID-4.7 scaffolds was 390±49 μm and 490±45 μm, respectively. No statistical difference in thickness was detected for the TIPS scaffolds before and after ES, demonstrating absence of a significant compression effect due to the ES process. The external ES layer in the ID-1.3 and the ID-4.7 scaffolds had a thickness of 73±26 μm and 253±60 μm, respectively. The two layers appeared to be firmly adhered to each other with no grossly visible delaminations (*i.e.*, disconnections larger than the average TIPS pore size; see, *e.g.*, Figure 2-C). The observed adherence between the layers was presumably due to the combined effects of the many localized fusions of the ES nanofibers with the pore walls of the TIPS scaffolds (Figure 2-D). The TIPS layers of the ID-1.3 scaffolds had pore sizes measuring 51±3 μm while for the ID-4.7 scaffolds the pore size was 123±20 μm. The pore size of the ES layer (for both scaffold sizes) was 5.1±3.2 μm while the diameter of the ES nanofibers was 743±201 nm.

3.2. Mechanical properties

All scaffolds exhibited anisotropy for supra-physiologic values of distension reached throughout the uniaxial testing. The circumferential properties were generally characterized by a lower slope (stiffness) and lower UTS compared to the longitudinal properties for all three scaffolds (Figure 4-A). In particular, TIPS and ES PEUU scaffolds exhibited different uniaxial properties with different shapes of the stress-strain curve. The TIPS curve had an almost linear behavior while the ES curve had a nonlinear trend more similar to native tissues. The uniaxial plot of the ES-TIPS PEUU scaffolds had a shape in between that for the TIPS and ES alone, suggesting a balanced contribution of the two components (Figure 4-A). Stress–strain relationships measured for the complete range of circumferential and longitudinal directions of the ES-TIPS ID-4.7 scaffolds are illustrated in Figure 4-B. The average thickness for the hSVs and pIMAs were 346±121 μm and 231±38 μm, respectively.

The circumferential and longitudinal UTS values were significantly different for the TIPS scaffolds ($p = 0.038$), but not for the ES scaffolds ($p = 0.21$; Figure 5-A). For the ES-TIPS, the circumferential UTS was significantly weaker than the longitudinal UTS (8.3±1.7 MPa vs 21.1±4.8 MPa, respectively; $p = 0.013$; Figure 5-A). The ES and ES-TIPS scaffolds were significantly stronger than the TIPS PEUU ($p < 0.001$), regardless of the direction (Figure 5-A). The ES-TIPS PEUU scaffolds were significantly stronger (*i.e*, circumferential UTS) than hSVs (3.7±2.0 MPa; $p = 0.02$), while not showing statistical differences when compared to pIMAs (10.4±7.1 MPa; $p = 0.4$; Figure 5-B).

The STF was not significantly different in the two directions for either the TIPS ($p = 0.59$), the ES ($p = 0.35$), or the ES-TIPS PEUU scaffolds ($p = 0.56$; Figure 5-C). However, the ES-TIPS scaffolds were significantly more distensible (*i.e.*, greater STF) than the two other

scaffolds (*e.g.*, circumferential STF = 5.3±0.5; p = 0.014; Figure 5-C). The circumferential STFs for the hSVs and pIMAs were significantly lower than the ES-TIPS scaffolds (1.7±0.7 and 1.5±0.2, respectively; $p < 0.001$; Figure 5-D).

The approximated elastic moduli were not significantly different in the two directions for TIPS (p = 0.41; Figure 5-E) and ES-TIPS (p = 0.23; Figure 5-E) scaffolds, but were significantly different for the ES PEUU scaffolds (*i.e.*, 1.4±0.4 MPa and 1.8±0.3 MPa, respectively; $p < 0.001$; Figure 5-E). The circumferential elastic modulus for the ES-TIPS was similar to that of the hSVs, but significantly higher than that of the pIMAs (1.4±0.4 MPa vs 0.4±0.2 MPa; p = 0.01; Figure 5-F).

The burst pressure for the ID-4.7 ES-TIPS PEUU scaffolds was not significantly different than those of either hSVs or pIMAs (Figure 6-A). Suture retention force for the ES-TIPS scaffolds was significantly higher only than that of pIMAs (3.4±0.3 N vs 1.0±0.3 N; $p < 0.01$; Figure 6-B), while the suture retention tension was similar for ES-TIPS scaffolds and native vessels (Figure 6-C).

Comparison of the pressure-diameter (P-D) relationships recorded over a physiological arterial pressure pulse for the ES-TIPS PEUU scaffolds and the native vessels are shown in Figure 6-D. The dynamic compliance for the ES-TIPS is significantly higher than that of hSVs but significantly lower than that of pIMAs (*i.e.*, $4.6\pm0.5\times10^{-4}$ $mmHg^{-1}$ vs $3.4\pm2.0\times10^{-4}$ $mmHg^{-1}$ and $11.2\pm6.0\times10^{-4}$ $mmHg^{-1}$; Figure 6-E), while this trend is inverted for the dimensionless stiffness index β (Figure 6-F).

The percentage of variation of the initial, average external diameter over the pulse was plotted over 24 h of perfusion to demonstrate absence of plastic deformations of the scaffolds, which could possibly lead to dilations during sustained exposure to pulsatile arterial pressures. Though a trend existed to a very slight dilation (<1% over 24 h), the diameter at the end of the 24 h was not significantly different from that recorded at the beginning (Figure 7-A). Compliance also did not change significantly over 24 h from its initial value (Figure 7-B). Similarly, the dimensionless stiffness index β did not change significantly over the 24 h perfusion, with an initial value of 21.6±2.9 (Figure7-C).

3.3. Cell seeding

After seeding (following 2 h of static culture), fluorescent staining showed high cellular density inside the internal TIPS layer for both the ID-1.3 and ID-4.7 constructs (Figure 8). Cell distribution was qualitatively uniform across the entire thickness (radial direction) of the internal layer of the TEVG, and throughout the circumferential and longitudinal direction (data not shown). As designed, the external ES layer did not show the presence of cells due to its small, restrictive pore size avoiding passive cell penetration. Cell seeding efficiency in the ID-4.7 and ID-1.3 scaffolds was 91.3±1.6% and 93.2±1.7%, respectively. The seeding procedure took 1.5 min for the ID-1.3 scaffolds and 5 min for the ID-4.7 ones.

3.4. Dynamic cell culture

The 1.3-ID ES-TIPS scaffolds were highly cellularized immediately after seeding (Figure 9-A), confirming the results previously obtained with the same cell type and scaffold (recall Figure 8-B). After 3 days of dynamic culture, the constructs had a significant reduction in cell number followed by a non-significant variation at 7 days (Figure 9-B-D). After 3 and 7 days, some luminal areas presented multilayered accumulations of cells, some of which were detached from the lumen (Figure 9-C). The spreading quantification over 7 days of dynamic culture showed a positive trend, though not significant, from an initial value of cell area of 201±13 μm^2 to a final value of 265 ±92 μm^2.

4. Discussion

The scaffold is one of the most critical components in tissue engineering, as it should provide a temporary structure and milieu for regeneration, *i.e.*, gradual replacement of the scaffold with native-like tissue. Furthermore, the scaffold should provide mechanical support to withstand physiologic conditions over an extended period of time. The matching of mechanical properties with those of native vessels is a critical requirement for any small-diameter vascular graft, as mechanical mismatch has been associated with perturbation in the local hemodynamics, establishing a basis for restenosis and graft failure [36].

Throughout the last two decades many endeavors have been made to develop a mechanically and functionally sound TEVG to replace or bypass arterial segments. Extensive research has been dedicated, in particular, to the development of scaffolds with the right combination and compromise of mechanical, structural, and biological properties suitable for cardiovascular applications. Different approaches have been explored for this purpose, spanning from biological materials [10, 11, 16] to completely synthetic materials with [37, 38] or without [39, 40] surface modifications or hybrid approaches [41]. Biological scaffolds (*e.g.*, collagen and fibrin gels) can exhibit an intrinsic capacity for biocompatibility and bioactivity; however, they have also been associated with suboptimal mechanical properties [42] and may have the potential for disease transmission and immunogenicity. Decellularized biological tissues tend to offer improved mechanical properties, however, incomplete removal of exogenous materials has been attributed to severe immunological reactions in early human clinical trials [43] and thus these scaffolds, while clearly promising, require significant care in their preparation and characterization. Moreover, the seeding of these scaffolds is not readily achievable owing to their low porosity. Synthetic scaffolds have the capacity of exhibiting tunable and reproducible properties. However, the most commonly used aliphatic polyesters such as poly(glycolic acid), poly(L-lactic acid), and their copolymers are generally much stiffer than native soft tissues and can, under some conditions, induce a transient inflammatory response due to the acidity of their degradation products [44]. Another common challenge in tissue engineering is the difficulty of obtaining highly bulk-cellularized scaffolds due to intrinsic scaffold limitations such as insufficient pore size or interconnectivity, or to inadequate seeding techniques [45].

In this work, we developed and tested a PEUU-based scaffold for vascular tissue engineering obtained by combining two previously developed PEUU-processing techniques: TIPS [24] and ES [25]. The biocompatibility, cell attachment, and tunability of degradation rate and mechanical properties for the PEUU were previously demonstrated [23]. Moreover, recent *in vivo* studies have shown how the same material did not produce a detrimental host inflammatory response due to its degradation products but rather fostered remodeling [46-49]. Morphologically, the scaffold was biomimetic, presenting two concentric layers with the highly cellularized, porous TIPS layer mimicking the functional *tunica media* and the fibrous, external ES layer acting as the adventitial layer providing mechanical support. We speculate that these features might be able to guide the process of neo-tissue formation toward native-like features upon remodeling *in vivo*. The firm adhesion between the two layers was likely produced by solvent bonding, in which partially wet fibers, resulting from the short distance between nozzle and target (*i.e.*, 7 cm), attached to the TIPS layer during electrospinning. However, the firm adhesion between the two layers did not disrupt the interconnectivity between the pores across the thickness of the scaffold wall, as shown in Figure 2-D. This was indirectly demonstrated by the presence of a transluminal flow across the scaffold wall during cell seeding, which would have been denied by the presence of a “skin” produced as result of the electrospinning process. Mechanically, the ES-TIPS PEUU scaffolds showed sufficient strength for arterial vascular applications (*i.e.*, UTS, burst pressure, suture retention force) with physiologically-compatible values of elastic molulus,

compliance, stiffness, and suture retention strength when compared with hSVs or pIMAs, as well as with previously measured values for human arteries (burst pressure = 2031-4225 mmHg, suture retention force = 1.96±1.16 N) [14]. Furthermore, the ES-TIPS PEUU scaffold exhibited mechanical properties similar to those measured for healthy coronary arteries (compliance = $14.1\pm5.9\times10^{-4}$ $mmHg^{-1}$, beta stiffness = 16.9±7.1, elastic modulus = 1.4±0.72 MPa) [50]. These characteristics suggest that the ES-TIPS PEUU scaffold may represent an attractive substitute for matching the mechanical properties of native arteries. Indeed, in light of our previously demonstrated ability to reproducibly control the anisotropy of ES PEUU by varying the rotational speed of the mandrel [27], it is expected that a similar degree of control will be possible in the context of ES-TIPS PEUU scaffolds, thus potentially allowing for TEVG anisotropy to be tailored to that of the particular vessel targeted for replacement.

The ES-TIPS PEUU scaffolds maintained their geometry and mechanical properties over time while perfused *ex vivo* for 24 h with physiologic, pulsatile pressure waveforms. This feature may be critical for future *in vivo* application of the scaffold as a TEVG. Aneurysm formation, for example, is a possible drawback of TEVGs and may be due to the intrinsic viscoelastic behavior of thermoplastic polymers (creep) and weakening associated with degradation kinetics. The relatively slow *in vitro* degradation previously reported for PEUU [23] would likely help the host remodeling mechanisms to gradually replace the scaffold with native tissue while the scaffold provides mechanical integrity over an extended period of time. The presence of progenitor cells into the scaffolds might foster these remodeling mechanisms by producing signaling for both peri-anastomotic infiltration and proliferation of native vascular cells, as well as *in situ* colonization with blood circulating progenitor cells, as previously described [51]. *In vivo* studies for extended implant periods would be required to evaluate this concern. The ES-TIPS PEUU scaffolds were seeded with adult MDSCs which exhibit multipotentiality, self-renewal capabilities, and have a direct role in tissue remodeling and regeneration both *in vitro* and *in vivo* [30-32]. Furthermore, MDSCs might represent an ideal candidate for vascular applications as they can be easily harvested and expanded from a small striated muscle biopsy [52]. We have used MDSCs in our previous efforts toward the development of a viable TEVG and its culture *in vitro* [12], and to assess the efficiency of cell inclusion within a short seeding time in a study using a rotational vacuum seeding device [26]. A high cell density (~1.5×10^5 cells/mm^3) was obtained for both the ID-1.3 and the ID-4.7 scaffold sizes within a few minutes of seeding procedures and with high seeding efficiencies (>92%). These features are critical for the future clinical translation of TEVGs where rapid turnaround time is desired and wasting donor cells with inefficient seeding could be unacceptable.

By culturing the seeded scaffolds in dynamic conditions, it was possible to observe a significant cell loss between day 0 and day 3; however, the scaffolds still retained a good cell density and spreading throughout the wall (Fig. 9-B). This was likely caused by the elevated initial cell density used, which saturated the space pore available for cellular proliferation. Cells likely migrated toward areas of increased nutrient concentration (lumen), and then fell off the constructs, as suggested in Fig. 9-C. Therefore, further studies will be required prior to *in vivo* implantation, including different initial cell densities, and specific assays to cell quantify proliferation, viability, and possible apoptosis.

In previous studies we have assessed more extensive biological endpoints in TIPS-PEUU scaffolds, including cell viability, phenotype and ECM deposition following seeding and *in vitro* dynamic culture [12, 26]. While assessment of such endpoints in our compound ES-TIPS PEUU scaffold are clearly important prior to pre-clinical animal studies, the scope of the cell seeding studies conducted herein was intended to demonstrate feasibility, with the primary focus being mechanical characterization of the construct. Antithrombotic

assessment *in vitro* for both the bare and the MDSC-seeded scaffolds (*e.g.*, platelet adhesion quantification, *etc.*) has not been covered in the current study. However, bulk-seeding of MDSCs into the ES-TIPS scaffolds allows for an extensive cellular exposure onto the luminal surface of the scaffolds, as shown in Figs. 8 and 9. This observation, in combination with the recent finding that progenitor cells have an antithrombogenic function *in vivo* [53], suggests that the MDSC-seeded scaffolds might have antithrombogenic properties. The antithrombotic properties of the unseeded and seeded ES-TIPS scaffolds are being currently evaluated with *in vivo* studies in small and large animal models.

While the ES-TIPS PEUU scaffold exhibited material properties very similar to native arteries, these results were partially limited by a small percentage of the tests (*i.e.*, the uniaxial tensile testing performed to distinguish longitudinal from circumferential properties) performed in a dry state at room temperature and without cellular components for ease of testing, and by the assumption of incompressibility applied to the porous PEUU scaffolds. A dry testing condition is different from the one that the scaffold would experience when implanted *in vivo*, where the material would be hydrated, infiltrated with cells, at body temperature, and in contact with a complex biological milieu. It has been shown that the material properties of synthetic scaffolds might vary depending on the hydration conditions of the scaffold [54]. The reported differences in mechanical properties between dry and wet samples were relatively small. Therefore, testing in simplified environmental conditions might not significantly affect the mechanical properties of the scaffold reported here. Once implanted, the scaffold will undergo degradation and remodeling which will affect the mechanical properties over time. Ongoing studies will be necessary to quantify the performance of these scaffolds and their mechanical properties following *in vivo* remodeling. The assumption of incompressibility, while fully legitimate for the native blood vessels tested [55], might have introduced an underestimation in both compliance and uniaxial strength measurements. This assumption was used to maintain a consistent protocol while comparing PEUU scaffolds to native vessels, and was justified by the inherent safety factor introduced in the measurements as a result of such potential underestimation.

5. Conclusion

A tubular scaffold comprised of concentric TIPS and ES layers of an elastomeric polymer designed for vascular tissue engineering applications was described. A morphological and mechanical characterization showed similarities with native arterial structure, strength, and elasticity. The ES-TIPS PEUU scaffolds were shown to retain their geometry and properties upon short-term mechanical conditioning. We were able to efficiently seed and dynamically culture the scaffolds with adult stem cells, obtaining a densely cellularized TEVG within minutes and maintaining high levels of cellular content prior to a prospective implantation in an animal model. This combination of features might represent a step toward future clinical translation of TEVGs by providing a more suitable temporary support for the seeded and host cells to remodel into a native-like biologic vascular substitute.

Acknowledgments

The authors gratefully acknowledge the financial support of the United States National Institutes of Health through BRP grant number R01 HL069368 (to Drs. Wagner and Vorp). We thank Dr. Johnny Huard for supplying MDSCs, Dr. Marco Zenati and Dr. Takeyoshi Ota for supplying hSVs and pIMAs, Dr. Michael Sacks for the use of his uniaxial tensile testing apparatus, and Dr. Alejandro Nieponice, Dr. George C. Engelmayr, Jr., Douglas Chew, Donna Haworth, and Dr. Timothy Maul for their technical assistance.

References

[1]. Rosamond W, Flegal K, Friday G, Furie K, Go A, Greenlund K, et al. Heart disease and stroke statistics--2007 update: a report from the American Heart Association Statistics Committee and Stroke Statistics Subcommittee. Circulation. 2007; 115(5):e69–171. [PubMed: 17194875]

[2]. Onuma Y, Daemen J, Kukreja N, Serruys P. Revascularization in the high-risk patient: multivessel disease. Minerva Cardioangiol. 2007; 55:579–92. [PubMed: 17912164]

[3]. U.S. Renal Data System, USRDS. 2008 Annual Data Report: Atlas of Chronic Kidney Disease and End-Stage Renal Disease in the United States. National Institutes of Health, National Institute of Diabetes and Digestive and Kidney Diseases; Bethesda, MD: 2008.

[4]. Nowygrod R, Egorova N, Greco G, Anderson P, Gelijns A, Moskowitz A, et al. Trends, complications, and mortality in peripheral vascular surgery. J Vasc Surg. 2006; 43:205–16. [PubMed: 16476588]

[5]. Grigioni, M., et al. Vascular Grafts: Experiment and Modeling. WIT Press; Boston: 2003. Biomechanics and Hemodynamics of Grafting.

[6]. Basaran O, Karakayali H, Emiroglu R, Belli S, Haberal M. Complications and long-term follow-up of 4416 vascular access procedures. Transplant Proc. 2003; 35:2578–9. [PubMed: 14612024]

[7]. Xue L, Greisler HP. Biomaterials in the development and future of vascular grafts. J Vasc Surg. 2003; 37:472–80. [PubMed: 12563226]

[8]. Vorp DA, Maul T, Nieponice A. Molecular aspects of vascular tissue engineering. Front Biosci. 2005; 10:768–89. [PubMed: 15569617]

[9]. Wang XN, Chen CZ, Yang M, Gu YJ. Implantation of decellularized small-caliber vascular xenografts with and without surface heparin treatment. Artif Organs. 2007; 31:99–104. [PubMed: 17298398]

[10]. Grassl ED, Oegema TR, Tranquillo RT. A fibrin-based arterial media equivalent. J Biomed Mater Res A. 2003; 66:550–61. [PubMed: 12918038]

[11]. Seliktar D, Nerem RM, Galis ZS. Mechanical strain-stimulated remodeling of tissue-engineered blood vessel constructs. Tissue Eng. 2003; 9:657–66. [PubMed: 13678444]

[12]. Nieponice A, Soletti L, Guan J, Deasy BM, Huard J, Wagner WR, et al. Development of a tissue-engineered vascular graft combining a biodegradable scaffold, muscle-derived stem cells and a rotational vacuum seeding technique. Biomaterials. 2008; 29:825–33. [PubMed: 18035412]

[13]. Niklason LE, Gao J, Abbott WM, Hirschi KK, Houser S, Marini R, et al. Functional arteries grown in vitro. Science. 1999; 284:489–93. [PubMed: 10205057]

[14]. L'Heureux N, Dusserre N, Konig G, Victor B, Keire P, Wight TN, et al. Human tissue-engineered blood vessels for adult arterial revascularization. Nat Med. 2006; 12:361–5. [PubMed: 16491087]

[15]. Weinberg CB, Bell E. A blood vessel model constructed from collagen and cultured vascular cells. Science. 1986; 231:397–400. [PubMed: 2934816]

[16]. L'Heureux N, Paquet S, Labbe R, Germain L, Auger FA. A completely biological tissue-engineered human blood vessel. Faseb J. 1998; 12:47–56. [PubMed: 9438410]

[17]. Seifalian AM, Tiwari A, Hamilton G, Salacinski HJ. Improving the clinical patency of prosthetic vascular and coronary bypass grafts: the role of seeding and tissue engineering. Artif Organs. 2002; 26:307–20. [PubMed: 11952502]

[18]. Nerem RM, Seliktar D. Vascular tissue engineering. Annu Rev Biomed Eng. 2001; 3:225–43. [PubMed: 11447063]

[19]. Hubbell JA. Biomaterials in tissue engineering. Biotechnology (NY). 1995; 13:565–76.

[20]. Nerem RM. Role of mechanics in vascular tissue engineering. Biorheology. 2003; 40:281–7. [PubMed: 12454417]

[21]. Sarkar S, Lee GY, Wong JY, Desai TA. Development and characterization of a porous micro-patterned scaffold for vascular tissue engineering applications. Biomaterials. 2006; 27:4775–82. [PubMed: 16725195]

[22]. Xu C, Inai R, Kotaki M, Ramakrishna S. Electrospun nanofiber fabrication as synthetic extracellular matrix and its potential for vascular tissue engineering. Tissue Eng. 2004; 10:1160–8. [PubMed: 15363172]

[23]. Guan J, Sacks MS, Beckman EJ, Wagner WR. Synthesis, characterization, and cytocompatibility of elastomeric, biodegradable poly(ester-urethane)ureas based on poly(caprolactone) and putrescine. J Biomed Mater Res. 2002; 61:493–503. [PubMed: 12115475]

[24]. Guan J, Fujimoto KL, Sacks MS, Wagner WR. Preparation and characterization of highly porous, biodegradable polyurethane scaffolds for soft tissue applications. Biomaterials. 2005; 26:3961–71. [PubMed: 15626443]

[25]. Stankus JJ, Guan J, Wagner WR. Fabrication of biodegradable elastomeric scaffolds with sub-micron morphologies. J Biomed Mater Res A. 2004; 70:603–14. [PubMed: 15307165]

[26]. Soletti L, Nieponice A, Guan J, Stankus JJ, Wagner WR, Vorp DA. A seeding device for tissue engineered tubular structures. Biomaterials. 2006; 27:4863–70. [PubMed: 16765436]

[27]. Courtney T, Sacks MS, Stankus J, Guan J, Wagner WR. Design and analysis of tissue engineering scaffolds that mimic soft tissue mechanical anisotropy. Biomaterials. 2006; 27:3631–8. [PubMed: 16545867]

[28]. Stankus JJ, Guan J, Fujimoto K, Wagner WR. Microintegrating smooth muscle cells into a biodegradable, elastomeric fiber matrix. Biomaterials. 2006; 27:735–44. [PubMed: 16095685]

[29]. Stankus JJ, Soletti L, Fujimoto K, Hong Y, Vorp DA, Wagner WR. Fabrication of cell microintegrated blood vessel constructs through electrohydrodynamic atomization. Biomaterials. 2007; 28:2738–46. [PubMed: 17337048]

[30]. Deasy BM, Huard J. Gene therapy and tissue engineering based on muscle-derived stem cells. Curr Opin Mol Ther. 2002; 4:382–9. [PubMed: 12222876]

[31]. Lee JY, Qu Petersen Z, Cao B, Kimura S, Jankowski R, Cummins J, et al. Clonal isolation of muscle-derived cells capable of enhancing muscle regeneration and bone healing. The Journal of Cell Biology. 2000; 150:1085–1100. [PubMed: 10973997]

[32]. Qu-Petersen Z, Deasy B, Jankowski R, Ikezawa M, Cummins J, Pruchnic R, et al. Identification of a novel population of muscle stem cells in mice: potential for muscle regeneration. J Cell Biol. 2002; 157:851–64. [PubMed: 12021255]

[33]. Kwon IK, Kidoaki S, Matsuda T. Electrospun nano- to microfiber fabrics made of biodegradable copolyesters: structural characteristics, mechanical properties and cell adhesion potential. Biomaterials. 2005; 26:3929–39. [PubMed: 15626440]

[34]. Engelmayr GC Jr. Sacks MS. A structural model for the flexural mechanics of nonwoven tissue engineering scaffolds. J Biomech Eng. 2006; 128:610–22. [PubMed: 16813453]

[35]. Severyn DA, Muluk SC, Vorp DA. The influence of hemodynamics and wall biomechanics on the thrombogenicity of vein segments perfused in vitro. J Surg Res. 2004; 121:31–7. [PubMed: 15313372]

[36]. Chung J, Li JK. Hemodynamic simulation of vascular prosthesis altering pulse wave propagation. Conf Proc IEEE Eng Med Biol Soc. 2004; 5:3678–80. [PubMed: 17271091]

[37]. Gumpenberger T, Heitz J, Bauerle D, Kahr H, Graz I, Romanin C, et al. Adhesion and proliferation of human endothelial cells on photochemically modified polytetrafluoroethylene. Biomaterials. 2003; 24:5139–44. [PubMed: 14568430]

[38]. Rashid ST, Salacinski HJ, Button MJ, Fuller B, Hamilton G, Seifalian AM. Cellular engineering of conduits for coronary and lower limb bypass surgery: role of cell attachment peptides and pre-conditioning in optimising smooth muscle cells (SMC) adherence to compliant poly(carbonate-urea)urethane (MyoLink) scaffolds. Eur J Vasc Endovasc Surg. 2004; 27:608–16. [PubMed: 15121111]

[39]. Naito Y, Imai Y, Shin'oka T, Kashiwagi J, Aoki M, Watanabe M, et al. Successful clinical application of tissue-engineered graft for extracardiac Fontan operation. J Thorac Cardiovasc Surg. 2003; 125:419–20. [PubMed: 12579118]

[40]. Niklason LE, Abbott W, Gao J, Klagges B, Hirschi KK, Ulubayram K, et al. Morphologic and mechanical characteristics of engineered bovine arteries. Journal of Vascular Surgery. 2001; 33:628–38. [PubMed: 11241137]

[41]. Zhu Y, Gao C, He T, Shen J. Endothelium regeneration on luminal surface of polyurethane vascular scaffold modified with diamine and covalently grafted with gelatin. Biomaterials. 2004; 25:423–30. [PubMed: 14585690]

[42]. Cummings CL, Gawlitta D, Nerem RM, Stegemann JP. Properties of engineered vascular constructs made from collagen, fibrin, and collagen-fibrin mixtures. Biomaterials. 2004; 25:3699–706. [PubMed: 15020145]

[43]. Simon P, Kasimir MT, Seebacher G, Weigel G, Ullrich R, Salzer-Muhar U, et al. Early failure of the tissue engineered porcine heart valve SYNERGRAFT in pediatric patients. Eur J Cardiothorac Surg. 2003; 23:1002–6. discussion 1006. [PubMed: 12829079]

[44]. Yang S, Leong KF, Du Z, Chua CK. The design of scaffolds for use in tissue engineering. Part I. Traditional factors. Tissue Eng. 2001; 7:679–89. [PubMed: 11749726]

[45]. Li H, Friend JR, Yeo LY. A scaffold cell seeding method driven by surface acoustic waves. Biomaterials. 2007; 28:4098–104. [PubMed: 17588654]

[46]. Fujimoto KL, Guan J, Oshima H, Sakai T, Wagner WR. In vivo evaluation of a porous, elastic, biodegradable patch for reconstructive cardiac procedures. Ann Thorac Surg. 2007; 83:648–54. [PubMed: 17258002]

[47]. Fujimoto KL, Tobita K, Merryman WD, Guan J, Momoi N, Stolz DB, et al. An elastic, biodegradable cardiac patch induces contractile smooth muscle and improves cardiac remodeling and function in subacute myocardial infarction. J Am Coll Cardiol. 2007; 49:2292–300. [PubMed: 17560295]

[48]. Guan J, Fujimoto KL, Wagner WR. Elastase-sensitive elastomeric scaffolds with variable anisotropy for soft tissue engineering. Pharm Res. 2008; 25:2400–12. [PubMed: 18509596]

[49]. Hong Y, Fujimoto K, Hashizume R, Guan J, Stankus JJ, Tobita K, et al. Generating elastic, biodegradable polyurethane/poly(lactide-co-glycolide) fibrous sheets with controlled antibiotic release via two-stream electrospinning. Biomacromolecules. 2008; 9:1200–7. [PubMed: 18318501]

[50]. Tajaddini A, Kilpatrick DL, Schoenhagen P, Tuzcu EM, Lieber M, Vince DG. Impact of age and hyperglycemia on the mechanical behavior of intact human coronary arteries: an ex vivo intravascular ultrasound study. Am J Physiol Heart Circ Physiol. 2005; 288:H250–5. [PubMed: 15331362]

[51]. Heil M, Ziegelhoeffer T, Mees B, Schaper W. A different outlook on the role of bone marrow stem cells in vascular growth: bone marrow delivers software not hardware. Circ Res. 2004; 94:573–4. [PubMed: 15031269]

[52]. Yokoyama T, Pruchnic R, Lee JY, Chuang YC, Jumon H, Yoshimura N, et al. Autologous primary muscle-derived cells transfer into the lower urinary tract. Tissue Eng. 2001; 7:395–404. [PubMed: 11506729]

[53]. Hashi CK, Zhu Y, Yang GY, Young WL, Hsiao BS, Wang K, et al. Antithrombogenic property of bone marrow mesenchymal stem cells in nanofibrous vascular grafts. Proc Natl Acad Sci USA. 2007; 104:11915–20. [PubMed: 17615237]

[54]. Sell SA, McClure MJ, Barnes CP, Knapp DC, Walpoth BH, Simpson DG, et al. Electrospun polydioxanone-elastin blends: potential for bioresorbable vascular grafts. Biomedical Materials. 2006; 1:72–80. [PubMed: 18460759]

[55]. Girerd XJ, Acar C, Mourad JJ, Boutouyrie P, Safar ME, Laurent S. Incompressibility of the human arterial wall: an in vitro ultrasound study. J Hypertens Suppl. 1992; 10:S111–4. [PubMed: 1432310]

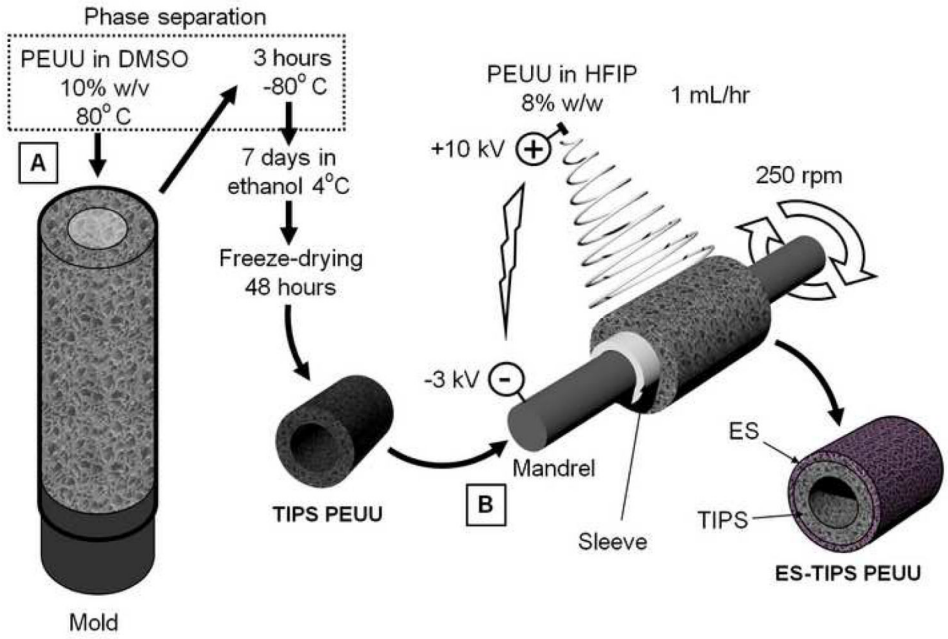

Figure 1.

ES-TIPS PEUU scaffold fabrication. **A.** The inner layer of the ES-TIPS PEUU scaffold is obtained by pouring hot polymer solution into a custom-made mold and rapidly freezing it to induce solvent-polymer phase separation (TIPS). **B.** After freeze drying, the resulting tubular scaffolds are mounted onto a mandrel in order to deposit an external micro-fibrous PEUU layer via electrospinning (ES). An intermediate sleeve between the TIPS scaffold and the mandrel is used to facilitate removal of the ES-TIPS scaffold at the end of the procedure.

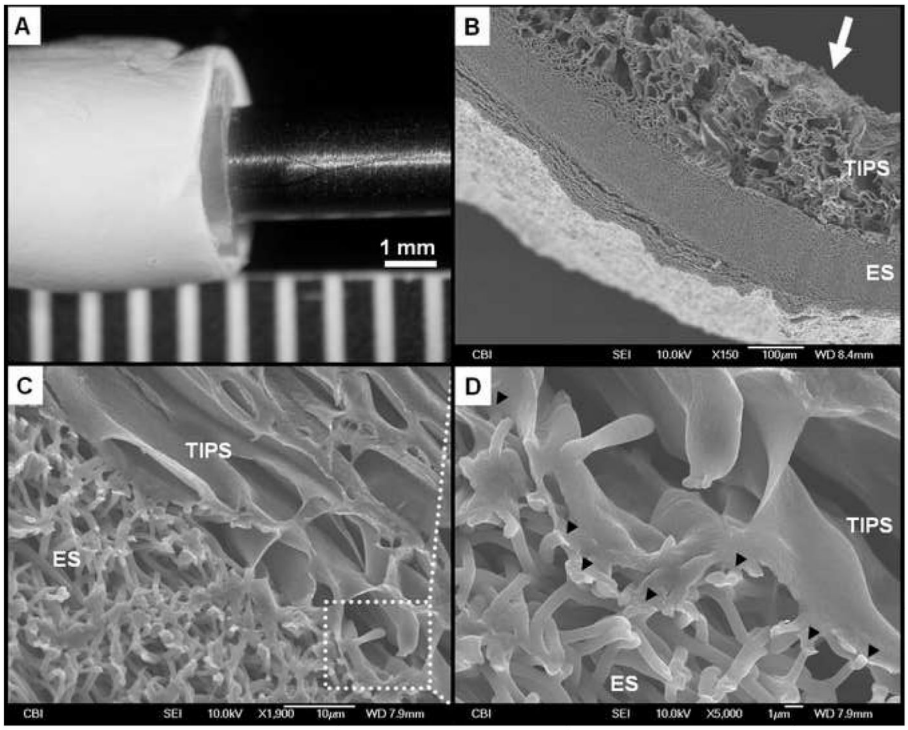

Figure 2.

Representative morphological assessment of the ID-4.7 ES-TIPS PEUU scaffold. **A.** Macroscopic appearance after electrospinning. **B.** Micrograph representing a cross-sectional portion of the compound scaffold. The arrow indicates the lumen. **C.** Interface between the two layers of the scaffold. **D.** Adhesion points (indicated by black arrow heads) in which electrospun fibers are fused with the pore structures of the TIPS.

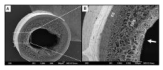

Figure 3.
Representative morphological assessment of the ID-1.3 ES-TIPS PEUU scaffold. **A.** Micrograph of the whole cross-section. Note the small luminal defect in the right portion of the scaffold due to sample processing (liquid nitrogen fracture). **B.** Increased magnification. The arrow indicates the lumen of the scaffold.

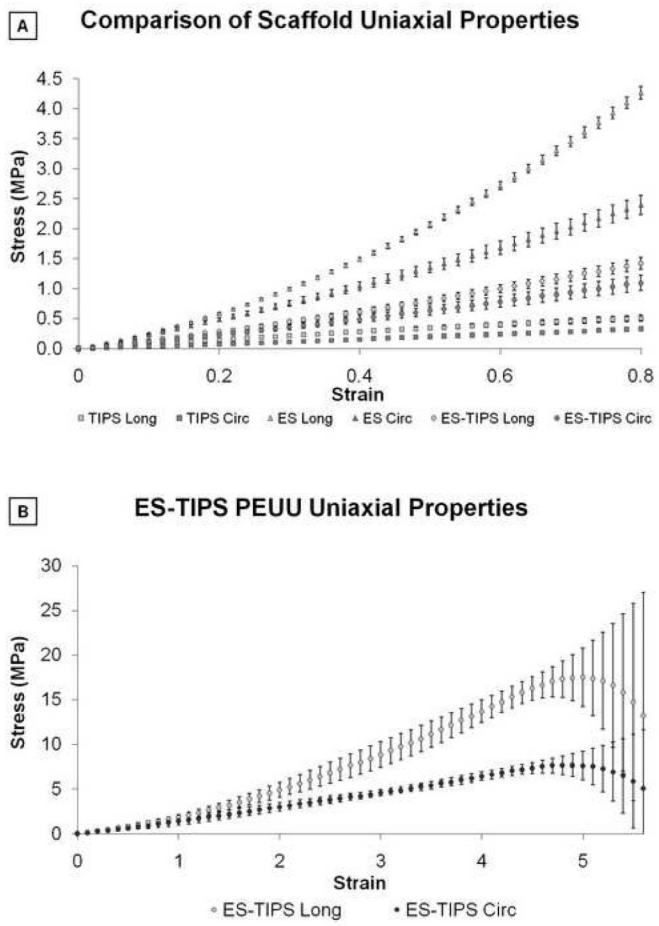

Figure 4.

Stress-strain plots from uniaxial tensile testing of PEUU scaffolds. **A.** Circumferential and longitudinal uniaxial tensile properties of ID-4.7 ES-TIPS PEUU scaffolds (circles) and its two single components (*i.e.*, TIPS PEUU (squares) and ES PEUU (triangles), respectively). Note the ES-TIPS material properties fall between those of its two individual components. (TIPS PEUU: n = 3; ES PEUU: n = 5; ES-TIPS PEUU: n = 3) **B.** Circumferential (dark grey) and longitudinal (light grey) uniaxial tensile properties of ID-4.7 scaffolds (mean ± standard deviation) along the complete testing range. The scaffold shows significant anisotropy ($p<0.05$; n = 3) with stiffer and stronger mechanical properties in the longitudinal direction. The level of strain to failure is comparable in the two directions. Note the level of breaking strain for the ES-TIPS scaffolds being approximately 500% of the initial sample length.

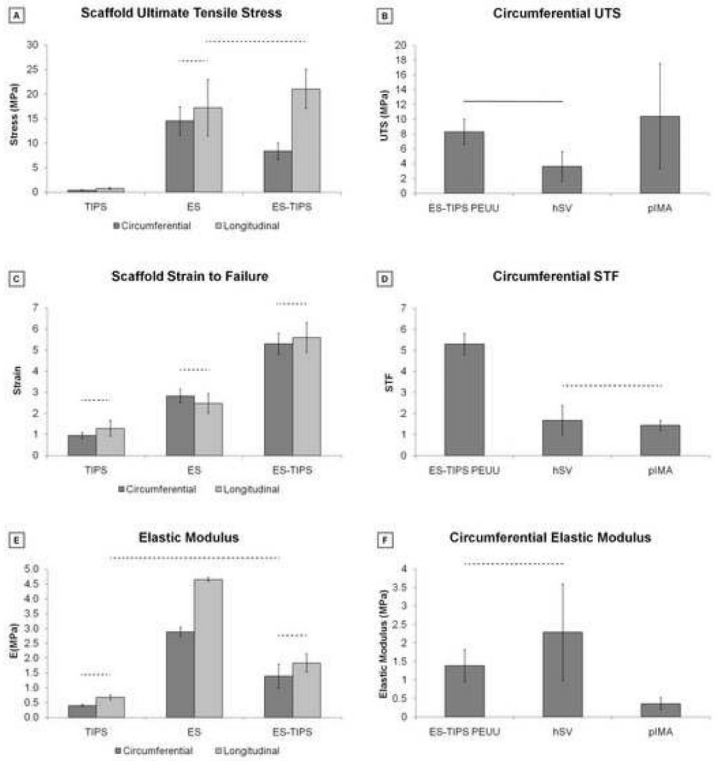

Figure 5.

Summary of mechanical properties based on uniaxial tensile testing of PEUU scaffolds and native blood vessels. **A.** Comparison of strength among the three different PEUU scaffolds. The dashed bars indicate the absence of statistical significance between two groups; all the other comparisons are statistically significant ($p < 0.05$) (TIPS PEUU: n = 3; ES PEUU: n = 5; ES-TIPS PEUU: n = 3). **B.** Comparison of circumferential UTS between ES-TIPS PEUU scaffolds and native vessels. The plain bar indicates statistically significant difference ($p < 0.05$) between two groups; all the other comparisons are not statistically significant. (ES-TIPS PEUU: n = 3; hSV: n = 4; pIMA: n = 6). **C.** Strain to failure results from uniaxial tensile tests for the three different PEUU scaffolds. **D.** Comparison of circumferential STF between ES-TIPS PEUU scaffolds and native vessels. **E.** Approximated elastic modulus for the three different PEUU scaffolds. **F.** Comparison of approximated circumferential elastic modulus between the ES-TIPS scaffolds and the native vessels.

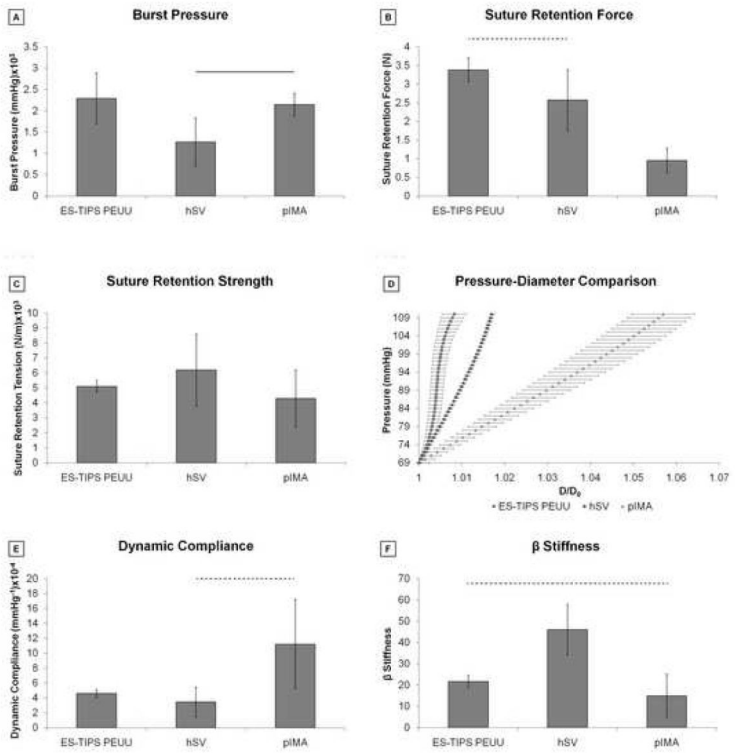

Figure 6.

Summary of mechanical properties based on pressurization of ES-TIPS scaffolds and native blood vessels. **A.** Comparison of burst pressure between ES-TIPS PEUU scaffolds and native vessels. The plain bar indicates statistically significant difference between two groups ($p < 0.05$); all the other comparisons are not statistically significant. (ES-TIPS PEUU: n = 3; hSV: n = 4; pIMA: n = 6). **B.** Comparison of suture retention force between the ES-TIPS PEUU and native vessels. The dashed bar indicates absence of statistically significant difference ($p < 0.05$) between two groups; all the other comparisons are statistically significant. **C.** Comparison of suture retention strength between ES-TIPS PEUU and native vessels. None of the differences are statistically significant. **D.** Comparison of P-D curves between ES-PEUU scaffolds and native vessels. These results are presented as average ± SEM. **E.** Comparison of dynamic compliance between ES-TIPS PEUU scaffolds and native vessels. **F.** Comparison of β stiffness between the ES-TIPS PEUU scaffolds and the native vessels.

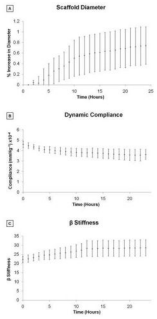

Figure 7.

Geometrical and mechanical properties of the ID-4.7 ES-TIPS PEUU scaffold measured throughout a 24 h period of perfusion under physiological arterial conditions presented as mean ± SEM; n = 3; no significant differences were detected between any time points). **A.** Percent variation of average external diameter from the initial value (*i.e.*, measured at time 0) for the ID-4.7 scaffold during perfusion *ex vivo*. **B.** Dynamic compliance. **C.** β stiffness.

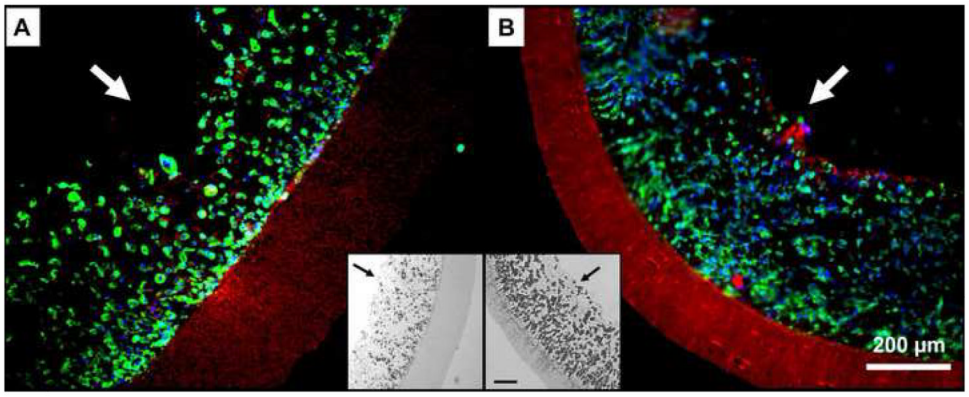

Figure 8.
Representative cell density of the ID-4.7 (**A**) and ID-1.3 (**B**) scaffolds 2 h after seeding (n=3). Blue=nuclei, green=F-actin, red=scaffold. **Insets.** Grayscale micrographs of the seeded scaffolds stained with H&E. Note the extent of the TIPS and ES layers. Scale bar = 100 μm. The arrows indicate the luminal surface of the scaffolds.

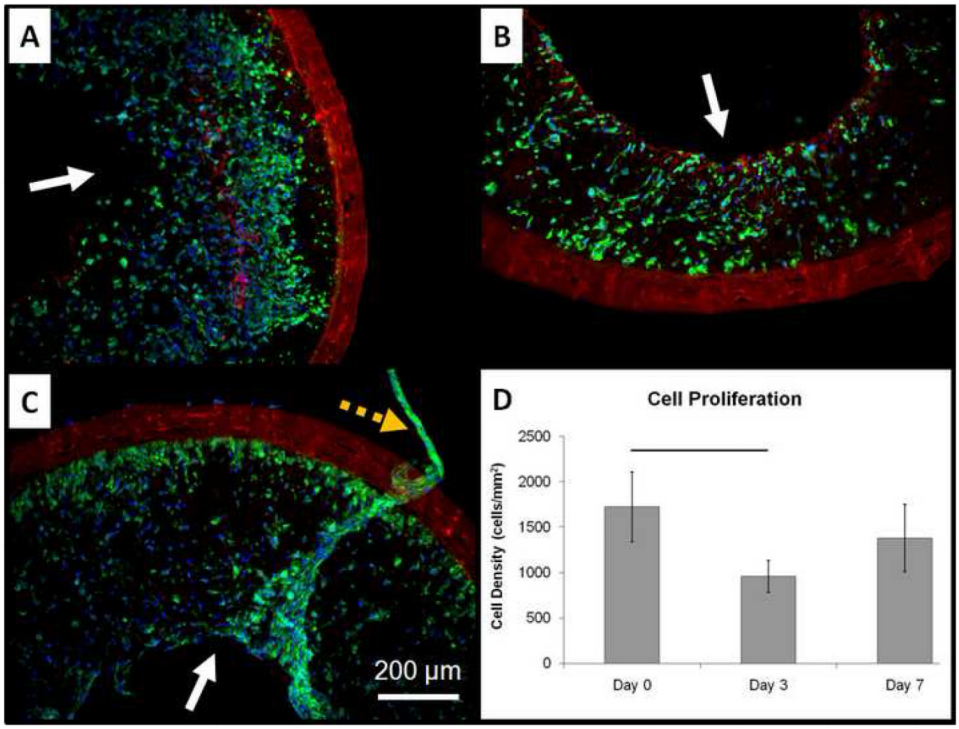

Figure 9.

Dynamic culture results for the rat MSCS-incorporated ID-1.3 ES-TIPS PEUU scaffolds. **A.** Representative qualitative results after 2 h of static culture. B. Results after 3 days of dynamic culture. C. Results after 7 days of dynamic culture. The plain arrows indicate the luminal surface. Blue = nuclei, green = F-actin, red = scaffold. Images taken at 100X. The dashed orange arrow indicates a tissue-like cluster of cells detaching from the luminar surface of the scaffold after 7 days of dynamic culture. **D.** Image-base quantification of cell density into ES-TIPS PEUU scaffolds at different time points. The bar indicates statistically significant difference between two groups ($p < 0.05$; $n = 3$); all the other comparisons are not statistically significant.